ORIGINAL ARTICLE

Design and Performance Study of an Ultrasonic Bone Scalpel with Composite Horn Structure

Jieping Wu[1,2] · Yong Yang[1,2] · Zhao Yang[1,2] · Cong Chen[1,2] · Shuai Huang[1,2]

Abstract

The ultrasonic bone scalpel was often used in all kinds of clinical orthopedic surgery as a new type of medical instrument. Based on the working theory of the ultrasonic bone scalpel and combined with the design method of a quarter wavelength transducer and horn, this study proposed an optimization design method for the ultrasonic bone scalpel with a composite horn structure. The structure of the ultrasonic bone scalpel was simplified, and its length was shortened. Finite element analysis, modal analysis, and harmonic response analysis were used to optimize the design of the ultrasonic bone scalpel. The performance of the ultrasonic bone scalpel was explored through impedance analysis, amplitude measurement, temperature measurement, and cutting tests, and the feasibility of the design was verified through torque analysis. The results showed that when the torque force was 4.0 N, the resonance frequency of the ultrasonic bone scalpel was 30,540 Hz, and the maximum amplitude of the ultrasonic bone scalpel could reach 62 μm. After spray cooling, the maximum surface temperature of the rear end cover was reduced from 51.8 to 36.3 ℃, the maximum surface temperature of the composite horn was reduced from 71 to 45.3 ℃, and the maximum surface temperature of the cutter head was reduced from 101 to 46.1 ℃, demonstrating a good cooling effect. Under 89 Voltage, the optimal cutting force for cutting chicken leg bones was 0.1 N, the optimal cutting force for cutting pork ribs was 0.3 N, and the cutting process showed tissue selectivity.

Highlights

1. Shorten the overall length of the ultrasonic bone scalpel, and design the overall length of the ultrasonic bone scalpel to half a wavelength.
2. Propose an optimization design method of ultrasonic bone knife with compound horn and compound horn structure.
3. Test the performance of the ultrasonic bone scalpel and complete the cutting experiments of the hard and soft tissue.

✉ Shuai Huang
huangshuai9228@126.com

1 College of Mechanical and Vehicle Engineering, Hunan University, Changsha 410082, China

2 National Engineering Research Center For High Efficiency Grinding, Hunan University, Changsha 410082, China

1 Introduction

In recent years, ultrasonic has developed rapidly and is widely used in cleaning [1], flaw detection [2], suspension [3], remote sensing [4], and other aspects. It also was rapidly developed in the medical industry. Cutting bone tissue is a kind of material removal process. The traditional bone scalpel is inefficient at cutting hard bone tissue, and the blade is easily worn, needing frequent replacement. The doctor has a long knife operation time, and the operation requirements are high. The ultrasonic bone scalpel is a new type of

medical instrument with the characteristics of high surgical accuracy, high efficiency, and less bleeding. It has tissue selectivity throughout the cutting process, does not damage peripheral nerve tissue, and has a fast postoperative recovery speed [5, 6]. Its clinical application is gradually increasing.

The structure of an ultrasonic bone scalpel is mainly composed of a transducer [7], a horn [8], and a knife. The transducer is mainly divided into the magnetostrictive transducer and the piezoelectric telescopic transducer. The piezoelectric telescopic transducer has the advantages of high electromechanical conversion efficiency, small volume, light weight, a wide trial frequency range, and so on. It is widely used in ultrasonic bone scalpels [9]. Its working principle is to use the inverse piezoelectric effect of piezoelectric ceramics to convert high-frequency electrical signals into mechanical vibration and transmit them to the front-end cover as the output amplitude of the ultrasonic transducer [10, 11]. The amplitude horn amplifies the transducer's amplitude and transmits it to the knife [12], causing the knife to generate high-frequency mechanical vibration. The ultrasonic energy of the knife is transmitted to the diseased tissue through contact to complete the cutting of the diseased tissue.

Through the mechanical effects and cavitation effects of the ultrasonic bone scalpel, it mainly completes the cutting of pathological tissue [13, 14]. The mechanical effect refers to the fact that when the ultrasonic bone scalpel contacts the diseased tissue, the high-frequency mechanical impact causes the protein hydrogen bond to break and is accompanied by heat generation [14–16] The cavitation effect refers to the fact that tiny bubbles or vacuoles will appear on the liquid–liquid surface and solid–liquid surface of pathological tissue when mechanical vibration is generated. Producing a strong destructive force and realizing the auxiliary cutting function when it is subjected to ultrasonic action, the vacuoles will quickly close or even collapse [14–16].

Scholars at home and abroad have optimized the structure of ultrasonic scalpels for various purposes. Kurosawa [17] developed a micro ultrasonic scalpel with a thickness of only 0.3 mm, which could be used in non-abdominal surgery or microsurgery together with an endoscope. Liu [18] designed an ultrasonic scalpel with a flexible end through mechanical vibration theory and an electromechanical equivalent method, which made the operation more flexible.

Finite element analysis is commonly used in designing the ultrasonic scalpel. De [19] established a multi-physical field finite element model to study the effects of mechanical vibration and mechanical cavitation of ultrasonic frequency on soft tissue. Ying [20] and others carried out finite element analyses on the cutting force and temperature of bone cutting. They comprehensively studied the effects of cutting speed, cutting depth, and vibration parameters (amplitude and frequency) on the cutting force and cutting temperature in the finite element model and discussed the mechanism of

the increase in cutting force and cutting temperature during bone cutting. In recent years, the performance comparison of similar devices is shown in Table 1.

Combining the quarter wavelength design method [7, 25] with numerical simulation and experiment, an optimization design method for the ultrasonic bone scalpel with composite horn structure was proposed in this paper. Finite element analysis, modal analysis, and harmonic response analysis were carried out to obtain the optimal mode and cutting amplitude of the ultrasonic bone scalpel. The effects of torque force, impedance analysis, amplitude measurement, temperature measurement, and cutting force on the performance of the ultrasonic bone scalpel were studied, and the feasibility of the design was verified. The results of this paper help simplify the structure of the ultrasonic bone scalpel and shorten its overall length.

Table 1 Performance comparison

Design frequency (kHz)	Output	Amplitude (μm)	No cooling operating temperature (°C)	Cutting material
28.9 [21]	30 W	–	–	Pig bone
40 [22]	100 W	110	–	Bone cement
55.5 [23]	–	40	–	–
73 [24]	20 V	5	–	–
271.9 [17]	20 V	0.6	–	Pork fat

2 Overall Design of the Ultrasonic Bone Scalpel

2.1 Transducer Design

The traditional ultrasonic bone scalpel was composed of a rear end cover, piezoelectric ceramic group, copper electrode piece, front-end cover, large horn end, and small horn end. According to the investigation, the type of piezoelectric ceramics, the matching degree of piezoelectric ceramics and design frequency, and the difficulty of obtaining materials, the design frequency of the ultrasonic osteotome was pre-selected as 30 kHz; the thickness of the piezoelectric ceramics was 2 mm, and the diameter was 10 mm. To ensure the consistency of the overall structure, the diameter of the front-end cover, the rear end cover, and the large end of the horn were 10 mm, and the areas were 78.5 mm². Because the amplification factor of the stepped horn was the largest, and considering the actual processing accuracy, the small end of the horn was 5 mm, and the small end section area was 19.6 mm².

Table 2 Material parameters of the transducer

Material	Density (kg/m^3)	Young's modulus (GPa)	Sound speed (m/s)	Wave number (rad/s)	Poisson's ratio
304 stainless steel	7850	205	5110	36.9	0.29
PZT-8	7600	–	2950	83.2	–
Titanium alloy	4940	105	4610	40.9	0.34

The total length of the ultrasonic bone scalpel was designed to be half a wavelength to realize the miniaturization and lightweight of the ultrasonic bone scalpel. Therefore, the quarter wavelength design method [7, 25] was adopted to design the total length of the ultrasonic transducer as a quarter wavelength. The calculation formula is shown in Formula (1).

$$\alpha_1 \frac{\rho_3 c_3 S_3}{\rho_2 c_2 S_2} \tan k_2 l_2 \tan k_3 l_3$$
$$+ \alpha_2 \frac{\rho_3 c_3 S_3}{\rho_1 c_1 S_1} \tan k_3 l_3 \tan k_1 l_1 \qquad (1)$$
$$+ \alpha_3 \frac{\rho_2 c_2 S_2}{\rho_1 c_1 S_1} \tan k_2 l_2 \tan k_1 l_1 = 1$$

where, ρ_1, ρ_2, ρ_3 are the material density of the front-end cover, the piezoelectric ceramic, and the rear end cover, respectively; c_1, c_2, c_3 are the longitudinal wave sound velocity of the front-end cover, the piezoelectric ceramic, and the rear end cover, respectively; S_1, S_2, S_3 are the sectional area of the front-end cover, the piezoelectric ceramic, and the rear end cover, respectively; k_1, k_2, k_3 are the wave number of the front-end cover, the piezoelectric ceramic, and the rear end cover, respectively; l_1, l_2, l_3 are the length of the front-end cover, the piezoelectric ceramic, the rear end cover, respectively; and α_1, α_2 and α_3 are correction coefficients that can be adapted according to design requirements.

The material of the rear end cover was 304 stainless steel because its large impedance can prevent the transmission of ultrasonic energy from the rear end cover. Because of high transmission power and good transmission performance, PZT-8 was selected as the piezoelectric ceramic material. The front-end cover was made of titanium alloy because it is bio-friendly and has low acoustic impedance, facilitating the transmission of ultrasonic energy to the horn and knife. The material parameters of each component are shown in Table 2.

First, the length of the rear end cover was determined. The length of the rear end cover was selected as 25, 26, 27, 28, 29, and 30 mm so that it is long enough to have a plane for clamping and fixing operations and is easy to hold. Based on the thickness of the piezoelectric ceramic chip group (8 mm), the length of the front-end cover was obtained through the calculation of the quarter wavelength

Table 3 Initial data of the transducer

Rear end cover (mm)	Piezoelectric ceramic group (mm)	Front-end cover (mm)
25	8	5.6
26	8	5.3
27	8	4.9
28	8	4.6
29	8	4.3
30	8	3.9

Table 4 Material parameters of the horn

Material	Density (kg/m^3)	Young's modulus (GPa)	Sound speed (m/s)	Wave number (rad/s)	Poisson's ratio
Titanium alloy	4940	105	4610	40.9	0.34

piezoelectric transducer (Formula (1)). The results are shown in Table 3.

2.2 Horn Design

A horn can be conical, exponential, stepped, or other structures. A stepped horn has a large amplification factor, so it was used, and the node was located at the wide end [26, 27]. This study aims to design an ultrasonic bone scalpel with a length of half the wavelength, and the length of the transducer was one-quarter the wavelength, so the horn was also one-quarter wavelength, and the calculation formula was shown in Formula (2). To ensure the consistency of ultrasonic energy transmission, titanium alloy was selected as the material of the horn, and its parameters are shown in Table 4.

$$\cot k_5 l_5 \cot k_4 l_4 = \frac{S_5}{S_4} \qquad (2)$$

where, k_4, k_5 are the wave number of the material at the large end and the small end of the horn, respectively; l_4, l_5 are

Table 5 Initial data of the horn

Large end of the horn (mm)	Small end of the horn (mm)
15	34.1
16	33.7
17	33.3
18	32.9
19	32.5
20	32.0

Table 6 The 30-mm combination table (mm)

Rear end cover	PZT-8	Large end of the composite horn	Small cylindrical end	Knife	Small end of the composite horn
30	8	18.9	7.1	27	34.1
30	8	19.9	6.7	27	33.7
30	8	20.9	6.3	27	33.3
30	8	21.9	5.9	27	32.9
30	8	22.9	5.5	27	32.5
30	8	23.9	5.0	27	32.0

Fig. 1 Structure of the ultrasonic bone scalpel. **a** Schematic diagram of the rear end cover, **b** Schematic diagram of a transducer, **c** Schematic diagram of the composite horn, **d** Schematic diagram of the cutter head, **e** Overall schematic diagram of the ultrasonic bone scalpel, **f** Specific structure of ultrasonic bone scalpel
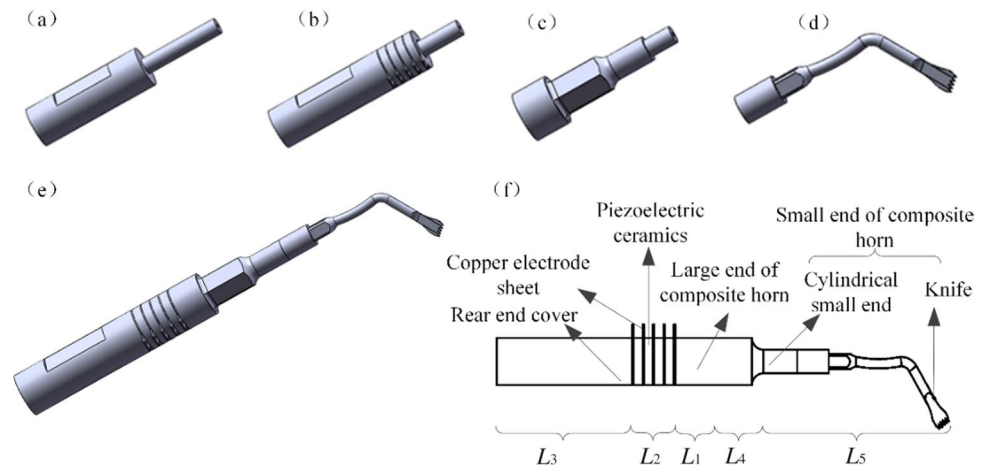
the length of the large end and the small end of the horn, respectively; S_4, S_5 is the sectional area of the large end and the small end of the horn, respectively.

In the same way, the length of the large end of the horn was determined. To facilitate assembly and avoid increasing the overall length of the ultrasonic bone scalpel, the length of the large end of the horn was initially set at 10, 11, 12, 13, 14, and 15 mm. The initial value of the small end of the horn was obtained through the calculation of the quarter wavelength stepped deformation horn (Formula (2)). The results are shown in Table 5.

2.3 Design of Ultrasonic Bone Scalpel With Composite Horn Structure

To simplify the structure, the ultrasonic bone scalpel was designed with a composite horn structure. The structure of the ultrasonic bone scalpel was improved based on the calculation in Tables 3 and 5. As shown in Fig. 1f, the lengths of the front-end cover (L_1) and the large end of the horn (L_4) jointly constituted the length of the large end of the composite horn. The length of the small end of the composite horn (L_5) was divided into two parts: the small cylindrical end and the knife. Thus, the length of the horn and the length of the

front-end cover were combined into a composite horn and a knife, thereby shortening the overall length of the ultrasonic bone scalpel. The knife was designed to be curved, and its total length was 27 mm. In the process of designing the composite horn, there are 36 random combination modes. Take the combination mode with the rear end cover length of 30 mm in Table 3 as an example and randomly combine it with the data in Table 5. The initial design data is shown in Table 6. The small cylindrical end needs to be long enough to ensure its close connection with the knife. Therefore, the selected length combination mode was as follows: The length of the rear end cover was 30 mm, the total thickness of the piezoelectric ceramic was 8 mm, the length of the large end of the composite horn was 18.9 mm, the length of the small cylindrical end was 7.1 mm, and the total length of the small end of the composite horn was 34.1 mm.

The final structure is shown in Fig. 1. Figure 1a is a schematic diagram of the rear end cover. The rear end cover was provided with a long stud on the end face to act as a central bolt to fix and connect the copper electrode sheet, piezoelectric ceramic group, and composite horn. To facilitate subsequent installation and disassembly, a flat position for clamping was arranged on the side of the rear end cover. Figure 1b is an assembly diagram of the rear end

cover, copper electrode sheet, and piezoelectric ceramic group. Figure 1c is the structural schematic diagram of the composite horn. Combined with Fig. 1, the composite horn was composed of two parts: the large end of the horn and the small cylindrical end. Studs were provided on the end face of the small cylindrical end. Meanwhile, the knife was designed independently to facilitate replacement and multiple functions. Simultaneously, the large end of the composite horn was set into an external hexagonal structure for fixing and disassembling. Figure 1d is a schematic diagram of the tool head. Internal threads were provided on the large end face of the tool head to cooperate with the studs on the small end face of the composite horn to facilitate the fixation and connection of the composite horn and the knife. Figure 1e is the overall assembly diagram of each part of the ultrasonic bone scalpel. Figure 1f shows the structure of the improved ultrasonic bone scalpel. The ultrasonic bone scalpel is composed of a rear end cover, piezoelectric ceramic group (four pieces), copper electrode sheet, composite horn, and knife. During the calculation, $L1$–$L5$ represents the lengths of the front-end cover, piezoelectric ceramic group, rear end cover, large end of the horn, and small end of the horn.

3 Structural Optimization of the Ultrasonic Bone Scalpel

3.1 Modal Analysis

The ultrasonic bone scalpel was modeled and analyzed using multi-physical field simulation software, and the rear end cover, piezoelectric ceramic group, and composite horn structure were drawn in the plane geometry module. To complete the contact and cooperation between the cutter head and the drawn figure, the geometric structure of the cutter head was drawn in the 3D modeling software and imported into FEM. The material parameters of each part of the ultrasonic bone scalpel are shown in Table 1. The free tetrahedral mesh was selected to divide the ultrasonic bone scalpel. Finally, the characteristic frequency, frequency domain, time domain, optimization, and other modules were added to analyze the ultrasonic bone scalpel.

The modes of the ultrasonic bone scalpel around 30 kHz were obtained using the modal analysis of the multi-physical field simulation software. Each modal diagram of the ultrasonic bone scalpel is shown in Fig. 2 from the *YZ* and *XZ* directions. Among them, the scalpels at 24,466 Hz in Fig. 2a and 43,813 Hz in Fig. 2b are in a torsional mode. The ultrasonic bone scalpel transducer mainly produced radial expansion and contraction vibration, and the deformation at the large end of the composite horn was relatively serious. There was bending vibration in the *X*-axis direction at the
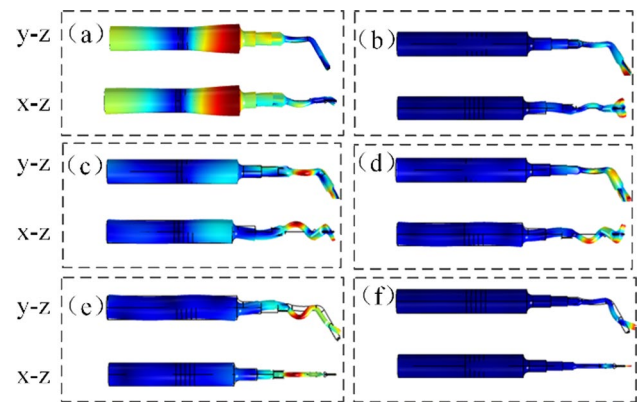

Fig. 2 Vibration mode deformation diagram of ultrasonic bone scalpels. **a** Torsion mode: 24,466 Hz, **b** Torsion mode: 43,813 Hz, **c** Bending mode: 26,423 Hz, **d** Bending mode: 33,147 Hz, **e** Bending mode: 33,849 Hz, **f** Longitudinal vibration mode: 30,110 Hz

small end of the composite horn. The vibration amplitude near the knife was small, mainly showing bending and torsional vibration around the *X*-axis.

The scalpels at 26,423 Hz (Fig. 2c), 33,147 Hz (Fig. 2d), and 33,849 Hz (Fig. 2e) are all in a bending mode. Those in Fig. 2c and Fig. 2d are bent in the *X*-axis direction, and the one in Fig. 2e is bent in the *Y*-axis direction. The vibrational deformation of the transducer part of the ultrasonic bone scalpel was small. The vibration deformation gradually increased at the large end of the composite horn, and serious bending vibration deformation occurred in the cylindrical section at the small end of the composite horn. The knife produced bending vibration in the radial direction of *X*-direction or *Y*-direction instead of the longitudinal vibration required.

The scalpel at 30,110 Hz in Fig. 2f is in a longitudinal vibration mode. The vibration of the transducer part of the ultrasonic bone scalpel and the large end of the composite horn was small, and the amplitude gradually increased along the direction from the composite horn to the knife and reached the maximum value near the knife. The knife vibrated back and forth in the *YZ* plane, and there was no bending or vibration in other directions in the *XZ* plane, indicating that the energy generated by the transducer was mainly transmitted to the tip of the knife, which promoted the longitudinal vibration of the cutter head.

3.2 Harmonic Response Analysis

After optimization analysis, the lengths of the rear end cover, the large end of the composite horn, the small cylindrical end, and the knife were finally determined to be 30, 17, 10 and 27 mm, respectively. Harmonic response analysis of the ultrasonic bone scalpel with longitudinal vibration mode was performed, and the results are shown in Fig. 3. A path was established at the center of the ultrasonic bone scalpel that penetrates
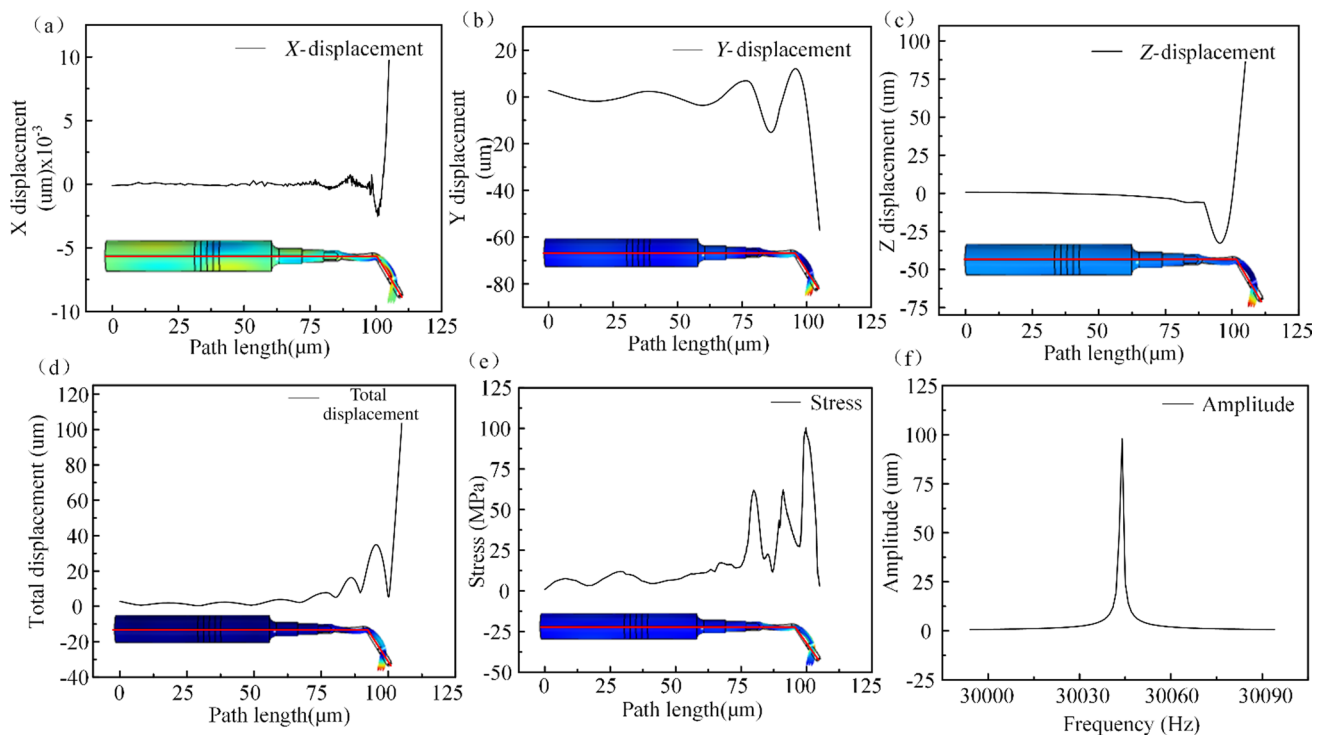
Fig. 3 **a** *X*-displacement distribution diagram. **b** *Y*- displacement distribution diagram. **c** *Z*-displacement distribution diagram. **d** Total displacement distribution diagram. **e** Stress distribution diagram. **f** Amplitude–frequency characteristic curve

from the rear end cover to the knife, and the displacement distribution and stress distribution of each particle position of the ultrasonic bone scalpel on the path were obtained. Figure 3a is the distribution diagram of the *X*-displacement component. The *X*-displacement of the rear end cover and the composite horn was small and almost unchanged. After passing the turning point of the knife, the *X*-displacement component began to rise gradually and reached the maximum value at the knife's tip, but its value was very small, and its impact on the ultrasonic bone scalpel could be ignored. Figure 3b is the distribution diagram of the *Y*- displacement component, showing that the *Y*- displacement component of the rear end cover and the large end of the composite horn was small and almost unchanged. The *Y*- displacement component gradually increased from the small end of the composite horn to its maximum value at the knife tip. Since the knife was curved, there was vibration in the *Y*-direction when the knife vibrated longitudinally, so the vibration met the requirements of longitudinal vibration. Figure 3c is the distribution diagram of *Z*-displacement components. From the figure, it can be seen that the *Z*-displacement components of the rear end cover and the large end of the composite horn are small, and the energy is mainly concentrated near the knife. The closer to the knife tip, the higher the amplitude, and the maximum value was obtained at the knife tip. The ultrasonic bone scalpel showed high-frequency vibration in the *YZ* plane.

Figure 3d is the path distribution diagram of the total displacement. The total displacement increased gradually along the direction from the rear end cover to the knife, and the maximum value was obtained at the knife tip. The small amplitude of the rear end cover and the large end of the composite horn indicated that the overall vibration amplitude of the ultrasonic bone scalpel was small and that the ultrasonic energy was mainly transmitted to the knife. Figure 3e is the stress distribution diagram. It could be concluded that the stress of the rear end cover and the large end of the horn was small, and the stress of the knife was large, indicating that the ultrasonic bone scalpel operated smoothly as a whole, and the knife was the main deformation and vibration part. Figure 3f is the amplitude–frequency characteristic curve. There were no other modes in the range of 30,000–30,100 Hz, and the amplitude reached its maximum value when the resonance frequency was 30,044 Hz.

4 Performance Testing of Ultrasonic Bone Scalpel

4.1 Torque Force Testing

On the basis of theoretical analysis and simulation optimization, the machining and assembly of the ultrasonic
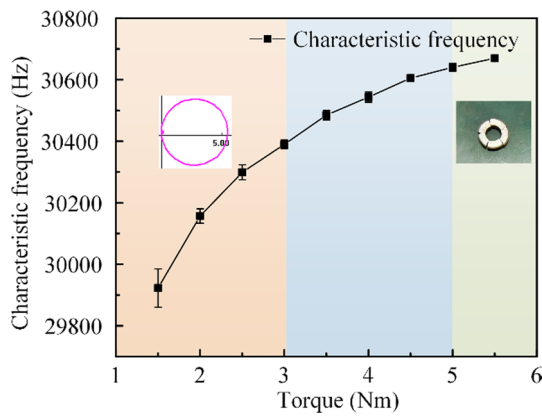
Fig. 4 Relationship between torque force and characteristic frequency
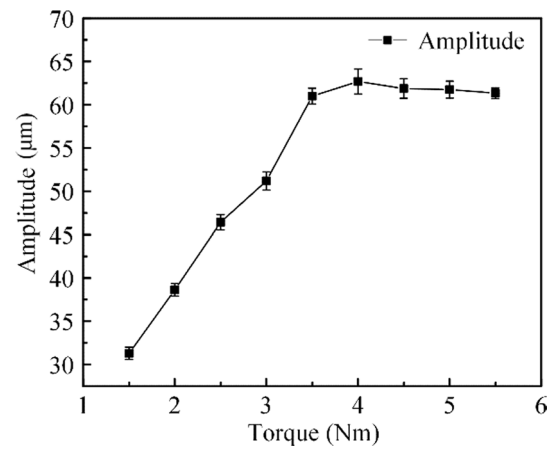

Fig. 5 Relationship between torque force and amplitude

bone scalpel were completed, and the torque force testing, impedance analysis, and amplitude measurement were carried out. Figure 4 shows the relationship between torque force and characteristic frequency. The scalpel's resonance frequency increased as torque increased, and the growth rate gradually slowed down and tended to be stable. When the torque force increased from 1.5 to 3 Nm, small dots appeared on the admittance circle. When the torque force was greater than 3 Nm, the small dots on the admittance circle began to disappear. When the torque force was greater than 5 Nm, the piezoelectric ceramics began to be squeezed and discharged, and partial or half of the piezoelectric ceramics even fragmented. This torsional torque was not suitable for the piezoelectric ceramics, so 4.0 Nm was selected as the final torsional torque. The reason for the above phenomena was that a small torque and incomplete contact between the components led to the origin of small dots on the admittance circle during impedance matching. When the torque was too large and exceeded the pressure tolerance range of piezoelectric ceramics, it was easy to deform, discharge, and break.

Figure 5 shows the relationship between the magnitude and amplitude of the torque force. It can be seen from the figure that with the increase of the torque force, the amplitude of the ultrasonic bone scalpel increased first and then remained unchanged. When the torque force was less than 3.5 Nm, the parts of the ultrasonic bone scalpel did not achieve close contact. The vibration was mainly transmitted through the stud, and there was energy loss; amplitude increased with the increase of the torque force, from the initial 31 to 61 μm. When the torque force was greater than 3.5 Nm, the parts of the ultrasonic bone scalpel were in close contact. The vibration was mainly transmitted through the contact surface and the stud. The energy transfer efficiency remained unchanged as the torque force increased, so the amplitude of the ultrasonic bone scalpel remained basically unchanged at around 62 μm.
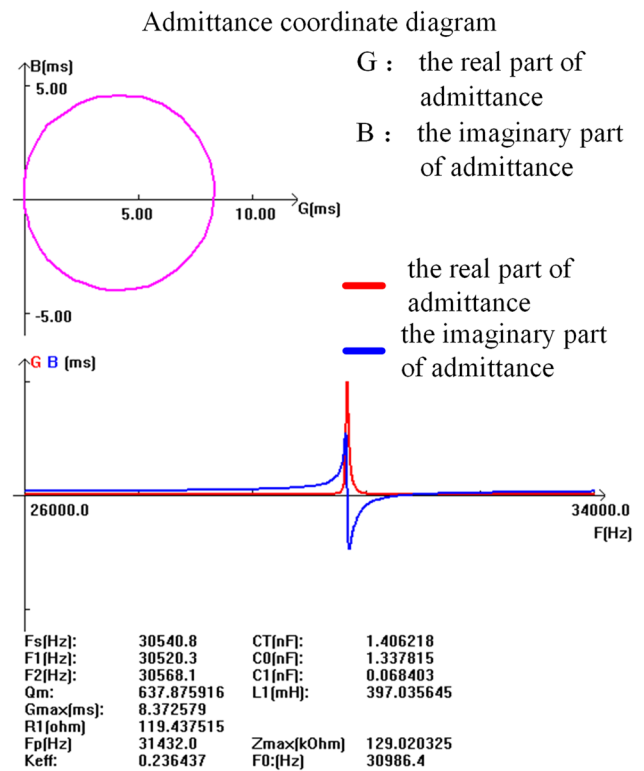

Fig. 6 Impedance analysis diagram

4.2 Impedance Analysis

Figure 6 shows the impedance analysis result of the ultrasonic bone scalpel. The resonant frequency was 30,540 Hz, which was consistent with the simulation analysis frequency of 30,044 Hz, with an error of 1.6%. The admittance graph had no parasitic circles or small spots, and there was only one peak in the logarithmic graph in the range of 26–34 kHz,
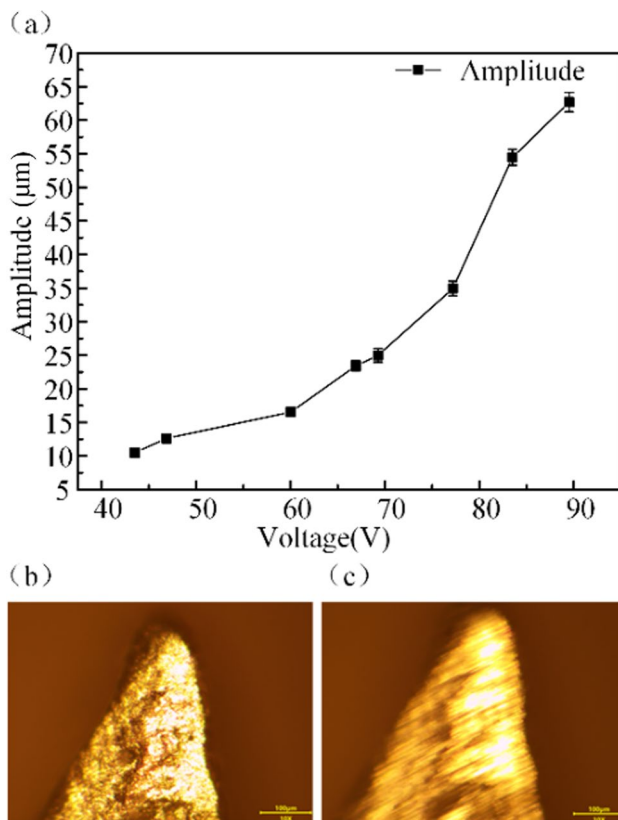
Fig. 8 Voltage variation trend with time

Fig. 7 Amplitude measurement diagram group. **a** Diagram of the relationship between voltage and amplitude. **b** Static diagram of amplitude measurement. **c** Dynamic diagram of amplitude measurement

which was consistent with the modal analysis in the simulation analysis, indicating that there was no interference from other models around and the vibration performance was stable.

4.3 Amplitude Measurement

Figure 7a shows the relationship between voltage and amplitude. The amplitude of the ultrasonic bone scalpel was measured using a Phoenix microscope. After the ultrasonic bone scalpel was enlarged by 100 times, the static and dynamic images shown in Figs. 7b, c were obtained. The amplitude of the ultrasonic bone scalpel tip could be converted based on the residual image range and scale size of the dynamic image of the ultrasonic bone scalpel. The results showed that the amplitude of the ultrasonic bone scalpel tip gradually increased with the increase in voltage. When the voltage was 89 V, the ultrasonic bone scalpel tip obtained a maximum amplitude of 62 μm, which was slightly different from 82 μm in the z-direction in the simulation analysis. It was speculated to be caused
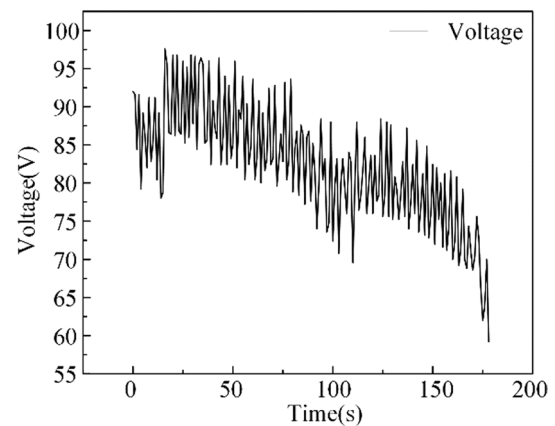
by simulation model simplification, machining error, and measurement error.

It should be noted that the voltage measured in Fig. 7 is the initial working voltage of the ultrasonic bone scalpel. The voltage fluctuated all the time. The fluctuation is shown in Fig. 8. The voltage on both sides of the ultrasonic bone scalpel decreased slowly with the extension of the working time. Because the piezoelectric ceramic was capacitive, there was a charge and discharge phenomenon, and the working temperature gradually increased, affecting the performance of the piezoelectric ceramic and causing the measured voltage value to decrease.

4.4 Cutting Experiment

Using chicken leg bones and pork ribs as the test materials, the relationship between the cutting force and the single hole cutting width was explored. The AUTODA AT8106 force sensor was used to measure the cutting force. The sensor was placed on the horizontal working surface and covered with a layer of a flat plate. The cut tissue was fixed on the flat plate, and the force at this time was calibrated as zero point. The tissue was cut with the ultrasonic bone scalpel, and a computer was used to obtain the data and control the force in real time. The final obtained cutting force is shown in Fig. 9, which is divided into five sections; the average value of each section is taken as the cutting force of this section, and the weighted average value of the cutting forces in all sections is taken as the cutting force of the cutting process.

The measurement results are shown in Figs. 10a, b. With the increase in cutting force, the cutting width of a single hole increased at first and then decreased. When the cutting force increased from 0 to 0.1 N, the single hole cutting width of chicken leg bone reached the maximum value of 0.66 mm, while when the cutting force continued to increase to 0.4 N, the single hole cutting width decreased from 0.66
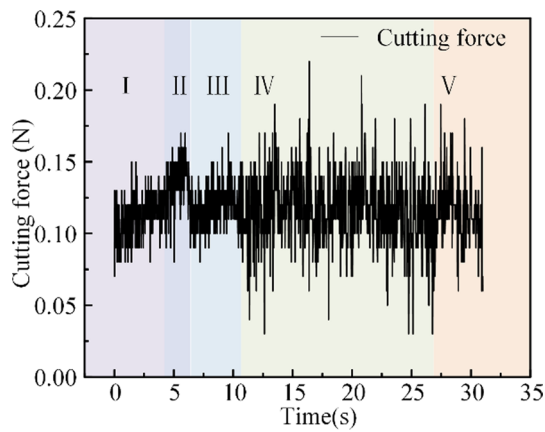
Fig. 9 Variation of cutting force

to 0.31 mm. When the cutting force increased from 0 to 0.3 N, the single hole cutting width of the pork ribs reached the maximum value of 0.4 mm, while when the cutting force continued to increase to 0.5 N, the single hole cutting width decreased from 0.4 to 0.23 mm. The difference in bone density and hardness between chicken legs bone and pork ribs led to different cutting force requirements and final single hole cutting widths. The cutting effect of the scalpel was closely related to the contact state of the knife and the material properties of the cut tissue. During the process, when the cutting width increased with the cutting force, the knife and the tissue changed from a non-contact state to a close contact state. The resistance of the knife was small, the high-frequency vibration could be maintained continuously, the energy transmission efficiency was high, the cutting quality was good, and the cutting width was gradually increased. When the cutting force continued to increase, the knife developed from the close contact state to the over-close contact state, increasing the resistance load on the knife, suppressing the high-frequency vibration effect, and reducing the energy transmission efficiency, surface cutting quality, and cutting width. Figure 10c shows the cutting morphology under the cutting force corresponding to Figs. 10a, b. It should be noted that in this cutting experiment, no cooling method was used, so the cut hole may be in a scorched state.

The cutting effect of the chicken leg bone, pork chop bone, and chicken meat are respectively shown in Figs. 10d, e, f. The knife was serrated, and the water-cooling method was adopted. When cutting force was applied at the same position, the knife formed multiple clear square cut marks on the chicken leg bone and pork chop bone; the incision was neat, and the cutting effect was remarkable. The scalpel did not show a good cutting effect on the chicken meant

Fig. 10 Cutting performance diagram group. **a** Relationship between cutting force and single hole width (chicken leg bone). **b** Relationship between cutting force and single hole width (pork ribs). **c** Cutting morphology of chicken leg bone (*left*) and pork ribs (*right*). **d** Chicken leg bone cutting photograph. **e** Pork ribs cutting photograph. **f** Chicken meat cutting photograph
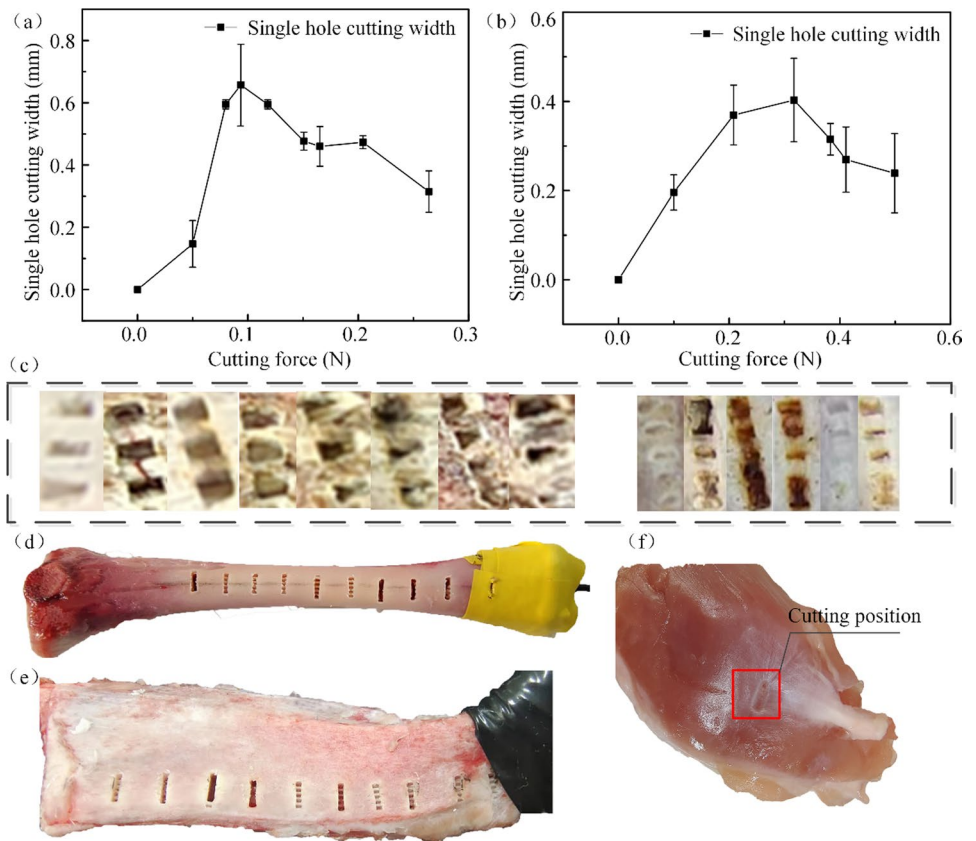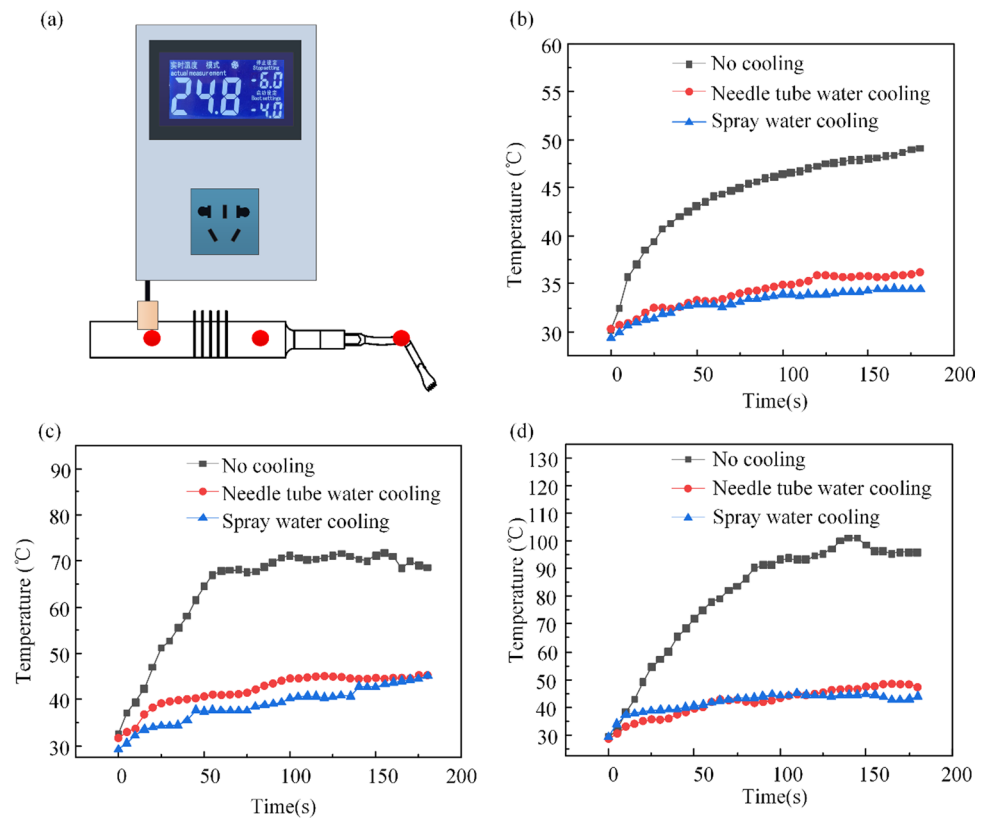
Fig. 11 Temperature measurement diagram group. **a** Schematic diagram of temperature measurement. **b** Temperature of the rear end cover. **c** Temperature of the composite horn. **d** Temperature of the knife

4.5 Temperature Measurement

Temperature was an important index for evaluating bone tissue damage. The temperature of bone tissue was directly affected by the temperature of the ultrasonic scalpel. The temperatures of each part were measured by contacting a microcomputer digital temperature controller probe, as shown in Fig. 11a, to the rear end cover, composite horn, and knife during operation. Simultaneously, three cooling methods, namely non-cooling, needle tube water cooling, and spray water cooling, were used to cool the ultrasonic bone scalpel to explore the cooling effect of different cooling methods. The results are shown in Figs. 11b, c, d. The temperatures were measured when the ultrasonic bone scalpel worked for 3 min. Under the condition of no cooling, the surface temperatures of the three parts first increased

and could only produce an indentation on it. Therefore, the scalpel is tissue-selective; it has a good cutting effect on "hard" tissues, such as chicken leg bone and pork ribs, and less damage to "soft" tissues, such as chicken meat and fat. Therefore, the ultrasonic bone scalpel causes little damage to surrounding nerves, blood vessels, and muscles in the process of cutting the bone. It can cut the diseased tissue accurately, improving safety and accelerating postoperative recovery.

and then gradually stabilized. The maximum temperature of the rear end cover, composite horn, and knife surfaces was 51.8, 71, and 101 ℃, respectively. The surface temperature of the ultrasonic bone scalpel was greatly reduced after needle tube water cooling or spray water cooling was adopted. The cooling effect of spray water cooling was better than that of needle tube water cooling. The surface temperature of the rear end cover was reduced from 51.8 to 36.3 ℃ using the needle tube water cooling method and further down to 34.7 ℃ when using the spray water cooling method. The surface temperature of the composite horn was reduced from 71 to 45.3 ℃ with the needle tube water cooling method and further down to 45℃ when using the spray water cooling method. The surface temperature of the knife was reduced from 101 to 46.1 ℃ using the needle tube water cooling method and further down to 42.8℃ when using the spray water cooling method.

5 Conclusions

In this study, the transducer and horn of the ultrasonic bone scalpel were designed preliminarily using the quarter wavelength design method, and an optimization design method for the ultrasonic bone scalpel with a composite horn structure was proposed. The overall structure was simplified into

three parts: the rear end cover, the composite horn, and the knife, shortening the length of the scalpel. Through numerical simulation analysis, the resonance frequency and mode of the scalpel were obtained. Torque analysis, impedance analysis, amplitude, temperature, cutting force, and other tests were performed after machining and assembly. The conclusions are as follows.

1. Through exploring the relationship between torque force and resonant frequency and amplitude, the optimal torque value was determined to be 4.0 Nm, and the maximum amplitude was 62 μm. The impedance analysis test revealed that the resonant frequency of the ultrasonic bone scalpel was 30,540 Hz.

2. The surface temperature of each part of the ultrasonic bone scalpel was measured under different cooling methods. The results showed that spray water cooling and needle tube water cooling could achieve significant cooling effects on each part of the ultrasonic bone scalpel, and the cooling effect of the former was better.

3. When cutting chicken leg bones, the cutting width of a single hole reached the maximum value of 0.65 mm under the cutting force of 0.1 N; when cutting pork ribs, the cutting width of a single hole reached the maximum value of 0.4 mm under the cutting force of 0.3 N.

Author contributions All authors read and approved the final manuscript.

Availability of Data and Material The authors declare that all data supporting the findings of this study are available within the article.

Declarations

Conflict of Interest The authors declare no potential conflicts of interest with respect to the research, authorship, and/or publication of this article.

References

1. Aktij SA, Taghipour A, Rahimpour A, Mollahosseini A, Tiraferri A (2020) A critical review on ultrasonic-assisted fouling control and cleaning of fouled membranes. Ultrasonics 108:106228

2. Guo C, Fang D, Wang CZ, Qin T, Liu ZH, Liu ZH, Zhang Y (2021) Ultrasonic flaw detection spectrogram characterization of vermicular graphite cast iron engine cylinder head. In: Journal of Physics: conference series (1)

3. Su QT, Li XD, Lu Y, Huang S (2022) Designing an ultrasonic array device to transport space particle suspension. J Adv Manuf Sci Technol. https://doi.org/10.51393/j.jamst.2022004

4. Legg M, Bradley S (2019) Ultrasonic arrays for remote sensing of pasture biomass. Remote Sens 12(1):111

5. He YY (2019) Clinical application of ultrasonic scalpel. Med Equip 06:192–193

6. Cao GK, Jiang XG, Bi PX, Qin W, Zhang DY (2016) The work mechanism and influence of force load on ultrasonic scalpel. Electromach Mould (01):44–46+58

7. Liu YY, Liu P, Chen XH, Sun FJ, Zhou HL (2022) Design and finite element analysis of sandwich transducer for ultrasonic scalpel. Nonferrous Metal Mater Eng 03:17–22

8. Wang R, Wang Y (2021) Design and finite element analysis of ultrasonic horn based on ABAQUS. Agric Equip Veh Eng 02:127–130

9. Liu ZH (2020) Study on vibration characteristics and cutting performance of ultrasonic bone scalpel. MA Thesis, Shandong University

10. Mei JL (2014) Investigation on PZT piezoelectric material d31 model series cantilever energy harvesting performance. MA Thesis, Xiangtan University

11. Wang T, Quan Q, Tang D, Yang Z, Deng Z (2021) Effect of hyperthermal cryogenic environments on the performance of piezoelectric transducer. Appl Therm Eng 193(3):116725

12. Cao FG (2005) Ultrasonic machining technology. Chemical Industry Press, Beijing

13. Lin GQ, Qu Z (2008) Application of ultrasonic scalpel in clinical surgery. Chin Med Equip J 08:108–109

14. Ellens N, Hynynen K (2015) High-intensity focused ultrasound for medical therapy. In: Power Ultrasonics, pp 661–693. Study on the Principle and Quality Control of Ultrasonic Scalpel

15. Zhao S, Jin C, Equipment DO, Society CW (2017) Study on the principle and quality control of ultrasonic scalpel. China Medical Devices

16. Suo JJ (2017) Thy study for vibration fatigue of ultrasonic scalpel. MA Thesis, Changchun University of Science and Technology

17. Kurosawa M, Umehara Y (2012) A micro ultrasonic scalpel with modified stepped horn. Electron Commun Jpn. https://doi.org/10.1002/ecj.10414

18. Liu HK (2017) Mechanism analysis and prototype design of ultrasonic scalpel with distal flexible joint. MA Thesis, Tianjin University

19. De S (2017) A multi-physics model for ultrasonically activated soft tissue. Comput Methods Appl Mech Eng. https://doi.org/10.1016/j.cma.2016.07.026

20. Ying ZZ, Shu LM, Sugita N (2020) Experimental and finite element analysis of force and temperature in ultrasonic vibration assisted bone cutting. Ann Biomed Eng 48(4):1281–1290

21. Zheng XT (2021) Design and experimental research of ultrasonic cambered bone cutting Device. MA Thesis, Sichuan University

22. Liu ZH, Sun CS, Cai CX, Zhang QH (2020) Integral design and simulation analysis of ultrasonic bone scalpel facing on human bone cutting. J Biomed Eng Res 39(1):6

23. Li X, Su C, Lin WJ (2019) Preliminary simulation and optimization design of ultrasonic harmonic scalpel. In: Symposium on piezoelectricity, acoustic waves and device applications (SPAWDA)

24. Sadiq M, Kuang Y, Cochran S, Huang Z (2015) High-performance planar ultrasonic tool based on d31-mode piezocrystal. Ultrason Ferroelectr Freq Control IEEE Trans 62(3):428–438

25. Yan CG, Shi Y, Yang L, Shi ZH, Li W, Yu W (2011) Design of quarter wavelength sandwich piezoelectric ceramic ultrasonic transducer. Tool Eng 03:72–74

26. Feng R (1999) Ultrasonics handbook. Nanjing University Press, Nanjing

27. Zuo YP (2016) The design and research of ultrasonic horn with longitudinal-torsion and flexural. MA Thesis, North China University of Technology
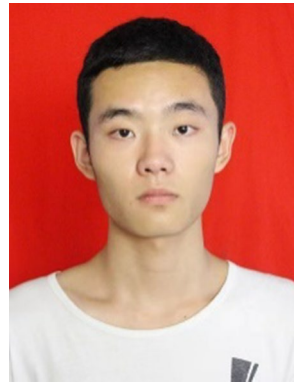
Zhao Yang is a postgraduate in College of Mechanical and Vehicle Engineering of Hunan University. His major research interest is the design of power supply for ultrasonic scalpel. He received Bachelor's degree in Xiangtan University in 2021.

Jieping Wu is a postgraduate in College of Mechanical and Vehicle Engineering of Hunan University. His major research interests are the design and performance testing of an ultrasonic bone scalpel. He received Bachelor's degree in mechanical engineering from China University of Petroleum-Beijing at Karamay in 2020.

Cong Chen is an assistant professor in College of Mechanical and Vehicle Engineering of Hunan University. He received his Ph. D. degree in Huazhong University of Science and Technology in 2017. He had been a postdoc in Huazhong University of Science and Technology from 2017 to 2019. His major research interests are focused on intelligent laser welding technology and equipment development.

Yong Yang is a postgraduate in College of Mechanical and Vehicle Engineering of Hunan University. His major research interest is acoustic levitation and transportation of ultrasonic array. He received Bachelor's degree in mechanical engineering from China University of Mining and Technology in 2020.

Shuai Huang is an associate professor in College of Mechanical and Vehicle Engineering of Hunan University. He received his Ph. D. degree in Dalian University of Technology in 2017. His major research interests are ultra-precision machining technology and equipment, medical devices and preparation and application of bionic functional surface.